NANO · MICRO small
www.small-journal.com

Hierarchical Micro- and Mesoporous Zn-Based Metal–Organic Frameworks Templated by Hydrogels: Their Use for Enzyme Immobilization and Catalysis of Knoevenagel Reaction

Kaipeng Cheng, Frantisek Svec, Yongqin Lv, and Tianwei Tan**

Encapsulation of enzymes in metal–organic frameworks (MOFs) is often obstructed by the small size of the orifices typical of most reported MOFs, which prevent the passage of larger-size enzymes. Here, the preparation of hierarchical micro- and mesoporous Zn-based MOFs via the templated emulsification method using hydrogels as a template is presented. Zinc-based hydrogels featuring a 3D interconnecting network are first produced via the formation of hydrogen bonds between melamine and salicylic acid in which zinc ions are well distributed. Further coordination with organic linkers followed by the removal of the hydrogel template produces hierarchical Zn-based MOFs containing both micropores and mesopores. These new MOFs are used for the encapsulation of glucose oxidase and horseradish peroxidase to prove the concept. The immobilized enzymes exhibit a remarkably enhanced increased operational stability and enzymatic activity with a k_{cat}/k_m value of 85.68 mM s^{-1}. This value is 7.7-fold higher compared to that found for the free enzymes in solution, and 2.7-fold higher than enzymes adsorbed on conventional microporous MOFs. The much higher catalytic activity of the mesoporous conjugate for Knoevenagel reactions is demonstrated, since the large pores enable easier access to the active sites, and compared with that observed for catalysis using microporous MOFs.

1. Introduction

Over the past several years, cell-free chemical biosynthesis using microbial cells with engineered pathways has emerged as a promising alternative for the biomanufacturing industry.[1–6] This new approach averts the tedious and challenging tasks to engineer and optimize synthetic pathways in live cells, and conquers the slow mass transfer controlled by both cell membranes and cellular processes.[7,8] Compared with in vivo synthesis, the cell-free systems enable the advantages of "plug-and-play" cascade assembly, diverse reaction conditions, as well as easy detection, separation, and purification of the products.[9] Cell-free biosynthesis utilizes in vitro networks comprising enzymes and cofactors, and facilitates inclusion of the separately produced enzymes into an optimal cascade. However, the use of free enzymes for industrial applications is often hampered by their limited operational stability as well as by difficulties with their recovery and recycling. Immobilization of soluble enzymes on solid supports is an effective strategy to overcome these limitations as it provides a number of benefits including enhanced enzyme stability, easy separation and recovery, and continuous use.[10–14] Considerable efforts have been invested in the development of scaffolds with controllable pore structures and surface properties in order to produce immobilized enzymes with enhanced stability while maintaining activity and selectivity.[15]

Metal–organic frameworks (MOFs) are highly crystalline hybrid inorganic–organic porous materials that are formed via assembling organic linkers with metal ion nodes or clusters.[16–19] Due to their distinct properties including uniform and controllable pore size and surface chemistry, ultrahigh surface area and porosity, as well as structural diversity, MOFs have sparked great interests and are instrumental in many applications including gas storage and separation,[20,21] separations and extractions in liquid phase,[22,23] catalysis,[24,25] sensors,[26] and biomedicine.[27] MOFs also feature a great potential as solid supports for immobilization of enzymes. Immobilization of enzymes in MOFs can be achieved via surface attachment, covalent linkage, coprecipitation, and pore entrapment.[15] The former two options in which enzymes were immobilized on the surface of MOFs via the formation of noncovalent interactions (van der Waals interaction, π–π stacking, or hydrogen bonds) or covalent bonds are the most straightforward.[28–30] However, these methods do not benefit from the porous properties of MOFs since the pores are not utilized. Coprecipitation is another strategy that includes immobilization of enzymes during the preparation of MOFs.[31–33] By embedding the enzyme in MOFs,

Dr. K. Cheng, Prof. F. Svec, Prof. Y. Lv, Prof. T. Tan
Beijing Advanced Innovation Center for Soft Matter Science and Engineering
Beijing University of Chemical Technology
Beijing 100029, China
E-mail: lvyq@mail.buct.edu.cn; twtan@mail.buct.edu.cn
Dr. K. Cheng, Prof. Y. Lv, Prof. T. Tan
Beijing Key Laboratory of Bioprocess
College of Life Science and Technology
Beijing University of Chemical Technology
Beijing 100029, China
The ORCID identification number(s) for the author(s) of this article can be found under https://doi.org/10.1002/smll.201902927.

DOI: 10.1002/smll.201902927

this scaffold can shield the enzymes and enhance their biological activity and long-term stability even under harsh conditions.[15,33–36] This technique is restrained to a limited number of MOFs that can be prepared under mild conditions. Another efficient strategy is encapsulation in pores in which enzymes diffuse into the pores of MOF.[37–40] This approach fully benefits from the presence of pores in MOFs and enables achieving high enzyme loading and reduces enzyme leaching. However, the widespread of this strategy was hampered by the small size of pore apertures common of most reported MOFs. The size most often smaller than 2 nm compares unfavorably with the larger enzyme molecules which size at least in one of the dimensions typically ranges in 3–5 nm. To overcome this limitation, design of new MOFs including mesopores enabling the effective immobilization of enzymes is highly desirable.

Ideally, MOF as an enzyme support should possess hierarchically porous structure with mesopores enabling enzyme immobilization connected through micropores for diffusion of substrate and product.[41–43] Methodologies including linker elongation, linker labilization, and linker thermolysis targeted this goal.[44–46] The templating is another type of efficient approach producing mesopores within MOFs framework such as double-solvent mediated overgrowth[47] and etching of nanoparticles.[48] To date, the reported templates include hexadecyl trimethyl ammonium bromide,[49,50] amphipathic surfactants,[51] block polymers,[52] poly(diallyldimethylammonium chloride),[53] and zinc hydroxide nitrate nanosheets.[54] Recently, Shen et al. pioneered the construction of MOF single crystals featuring highly oriented and ordered macropores using polystyrene nanosphere monolith as the template.[55]

We are now reporting a new, simpler, green, and easily manageable templating strategy for the preparation of hierarchical micro- and mesoporous zeolite imidazole frameworks HZIF-8 and HZIF-67 using hydrogel as the template. The hydrogel template was generated via the formation of hydrogen bonds between melamine and salicylic acid. The removal of hydrogel template at higher temperatures then produced mesopores within the ZIF framework. As the proof of concept, we co-encapsulated two model enzymes, glucose oxidase (GOx) and horseradish peroxidase (HRP) and demonstrated that the enzymes immobilized within HZIF exhibited a higher catalytic efficiency and operational stability compared to both enzymes immobilized in conventional microporous ZIF and enzymes in solution. HZIFs were also significantly more active catalyst compared with microporous ZIFs in the Knoevenagel reactions due to the presence of mesopores that facilitated mass transfer of both substrates and products.

2. Results and Discussion

2.1. Creating Hierarchical Mesopores in ZIFs Using Hydrogel as Template

Our new strategy relied on the preparation of the hierarchical micro- and mesoporous HZIFs via the templated emulsification method using hydrogel as the template (**Scheme 1**). Melamine and salicylic acid were selected as the templating agents for the following reasons: (i) The hydrogel can be formed via the self-assembly of melamine and salicylic acid upon cooling of their hot solution facilitated through the hydrogen bonds, (ii) the hydrogel template can be easily removed after its decomposition at a temperature increase to 75 °C, and (iii) melamine and salicylic acid coordinate with metal ions serving as seeds for the further growth of MOFs. The two-component hydrogel was obtained from the standard heating–cooling approach in aqueous medium via the formation of hydrogen bonds between melamine and salicylic acid. The coordinating interaction between the MOF precursor and hydrogel is critical for the successful formation of mesoporous MOFs directed by the 3D interconnecting network of hydrogel. Both melamine and salicylic acid function not only as the template but also as the coordinating agents that are chemically attached to the metal precursor during the self-assembling process.

Zeolitic imidazolate framework-8 (ZIF-8, $Zn(Hmim)_2$; Hmim = 2-methylimidazolate) was first selected from the group of MOFs for the development of the hydrogel templating strategy due to its high stability in water and extensive applications as solid carrier for enzyme immobilization.[31,56–60] To create the hierarchically structured HZIF-8, zinc ions were first mixed with melamine and salicylic acid in water at a temperature of 75 °C to obtain a homogeneous solution. During this step, melamine and salicylic acid behave as the coordinating agents and interact with zinc ion. The melamine-salicylic acid hydrogel is then formed after cooling the solution to room temperature. We first optimized the zinc ion contents in the gel. Although a high zinc percentage is required to generate more ZIF-8 crystals, we found that a zinc concentration exceeding 0.1 mol L^{-1} prevented the production of continuous and homogeneous hydrogel (Figure S1, Supporting Information). Thus, a zinc ion concentration of 0.1 mol L^{-1} was used in the following experiments. At this stage, the hydrogel with a 3D interconnecting network was produced by the self-assembly of gelators through intermolecular hydrogen bonds in which zinc ions were well distributed. The scanning electron microscopy (SEM) image of the Zn xerogel at dry state featured a fiber-like morphology which was similar to that of precursor hydrogel prepared in the absence of Zn ions (Figure S2a,b, Supporting Information). Energy-dispersive X-ray spectroscopy confirmed the uniform distribution of zinc in the

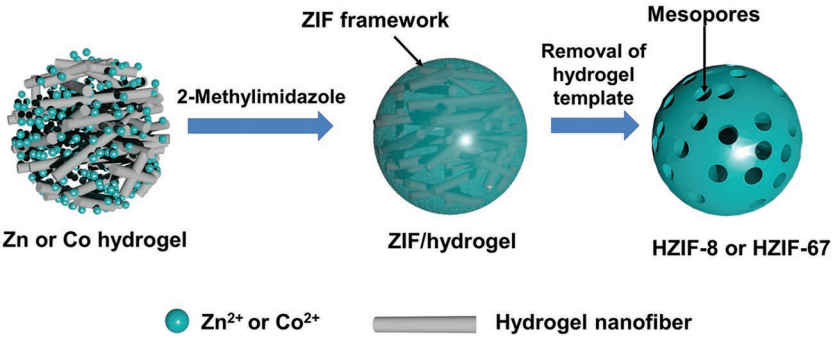

Scheme 1. Schematic illustration of the preparation of the hierarchical micro- and mesoporous zeolite imidazole frameworks (HZIFs) via a templated emulsification method with hydrogel used as the template.

xerogel fibers (Figure S2c,d, Supporting Information) with a zinc content of 12.15 at%.

The hot Zn hydrogel solution was poured in hexane containing Span 85 surfactant and the Zn hydrogel nanoparticles were generated via water-in-oil emulsification using magnetic stirring at 600 rpm and 60 °C for 1 h. Span 85 is a typical surfactant used for this process and assisted the formation of emulsion with oil as the continuous phase and water as the dispersed phase. After introducing 2-methylimidazole in this emulsion, zinc ions in the hydrogel nanoparticles coordinated with the organic linker, and gradually formed ZIF-8 nanocrystals encapsulated within the hydrogel template. Hierarchically structured ZIF-8 (HZIF-8) nanoparticles with both micropores and mesopores were ultimately produced after removal of the hydrogel template by incubating the nanoparticles in water at 75 °C for 12 h. The HZIF-8 nanoparticles were collected by centrifugation, and the supernatant was analyzed by electrospray ionization mass spectrometry (ESI-MS). The ESI-MS spectra in Figure S3 (Supporting Information) confirmed the presence of salicylic acid and melamine indicating the successful removal of the hydrogel template. To further confirm the complete extraction of the hydrogel, the mesoporous HZIF-8 nanoparticles were digested using 100 µL acetic acid-D4 and 500 µL DMSO-D6 and subjected to ^{1}H and ^{13}C NMR measurements. The NMR spectra in Figure S4 (Supporting Information) displayed the prominent peaks of salicylic acid (^{1}H NMR, 7.84, 7.31, 6.79 ppm) and melamine (^{13}C NMR, 162.56 ppm) in HZIF-8 containing hydrogel template. In contrast, these peaks were completely absent in spectrum of HZIF-8 after stripping the hydrogel template, and only the characteristic peaks of 2-methylimidazole could be observed.

The SEM and transmission electron microscopy (TEM) images in **Figures 1**a and **2**a revealed the successful generation of monodispersed spherical HZIF-8 nanoparticles with

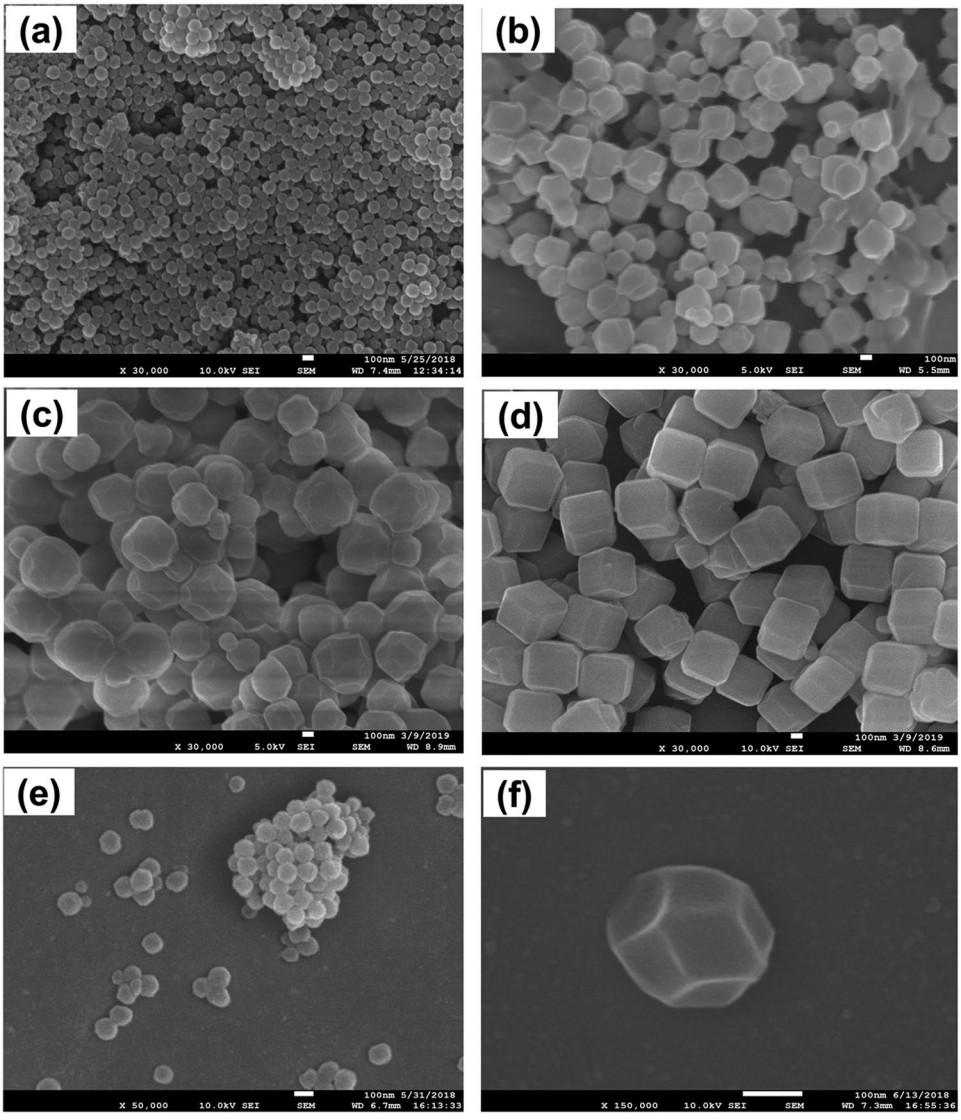

Figure 1. a–f) Scanning electron microscopy images of mesoporous HZIF-8 (0.1), microporous ZIF-8 prepared using conventional solvothermal method, mesoporous HZIF-8 (0.075), mesoporous HZIF-8 (0.05), mesoporous HZIF-67, and microporous ZIF-67 prepared using conventional solvothermal method.

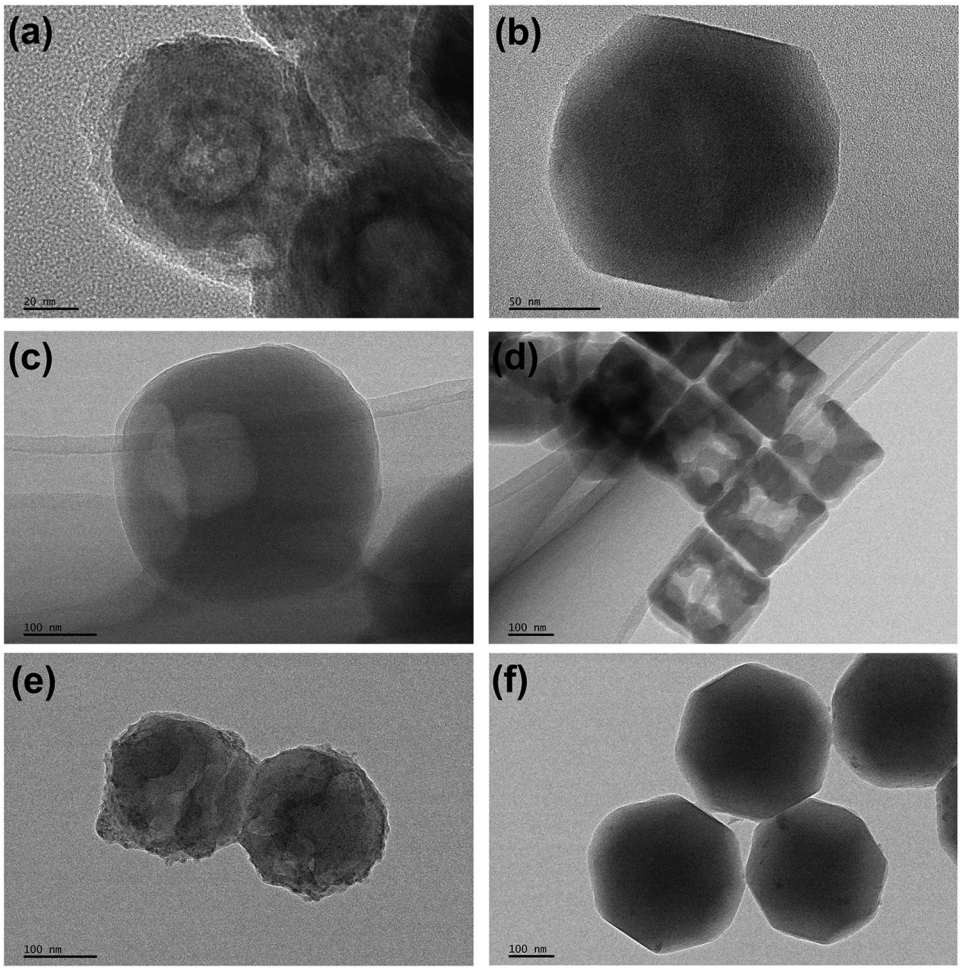

Figure 2. a–f) Transmission electron microscopy images of mesoporous HZIF-8 (0.1), microporous ZIF-8 prepared using conventional solvothermal method, mesoporous HZIF-8 (0.075), mesoporous HZIF-8 (0.05), GOx-HRP@HZIF-8(0.1), and GOx-HRP-on-ZIF-8.

remarkably uniform sizes, which were different from the typical rhombic dodecahedra morphology of ZIF-8 shown in Figures 1b and 2b that was prepared using conventional solvothermal method. The average particle size was 122 nm determined by dynamic light scattering (**Figure 3**a). This value was consistent with that observed in the SEM image. The powder X-ray diffraction (PXRD) patterns of Figure 3b confirmed the high crystallinity of HZIF-8 which matched well the conventional ZIF-8. No peaks were observed in the XRD patterns of both ZIF-8 and HZIF-8 below 5° (Figure S5, Supporting Information). The Fourier transform infrared (FTIR) spectrum of HZIF-8 in Figure 3c also matched that of the conventional ZIF-8 in which the characteristic peaks at 3135 and 2929 cm^{-1} were ascribed to the aromatic and aliphatic C—H stretching of imidazole groups. The band at 1584 cm^{-1} was attributed to the C=N stretching, whereas the prominent peaks at 1350–1500 cm^{-1} were assigned to the entire ring stretching. While the peaks centered at 900–1350 cm^{-1} belonged to the in-plane bending of the ring, those below 800 cm^{-1} were attributed to the out-of-plane bending. Notably, we also observed the characteristic peak centered at 421 cm^{-1} that belonged to the Zn—N stretching indicating the successful formation of ZIF-8 framework.[61] Due to the formation of hydrogen bonds in HZIF-8 containing the gel template, the $-NH_2$ stretching vibration peak at 3469 cm^{-1} of melamine shifted to higher energy of 3427 cm^{-1}, and the peak of the phenolic—OH group of the salicylic acid at 3389 cm^{-1} was totally lost.[62] Comparing the FTIR spectra of HZIF-8 and its counterpart containing gel template, the intensity of the band at 3427 cm^{-1} significantly decreased confirming the removal of the gel template. Moreover, the N_2 adsorption/desorption isotherm of HZIF-8 was the type IV indicating the presence of both micropores and mesopores, whereas the conventional ZIF-8 contained only micropores as demonstrated with the type I isotherm (Figure 3d,e). The calculated pore size distribution also confirmed the successful formation of mesoporosity in HZIF-8 with an average mesopore size of around 16.2 nm and a mesopore volume of 0.57 mL g^{-1} for HZIF-8 (0.1). **Table 1** compares the surface areas and pore volumes of both HZIF-8 and conventional ZIF-8. The surface area of HZIF-8 (0.1) was 1431.4 m^2 g^{-1}, which was similar to the conventional ZIF-8 featuring a surface area of 1403.3 m^2 g^{-1}.

The properties of HZIFs-8 prepared from hydrogel solutions containing zinc at concentrations 0.05 and 0.075 mol L^{-1}

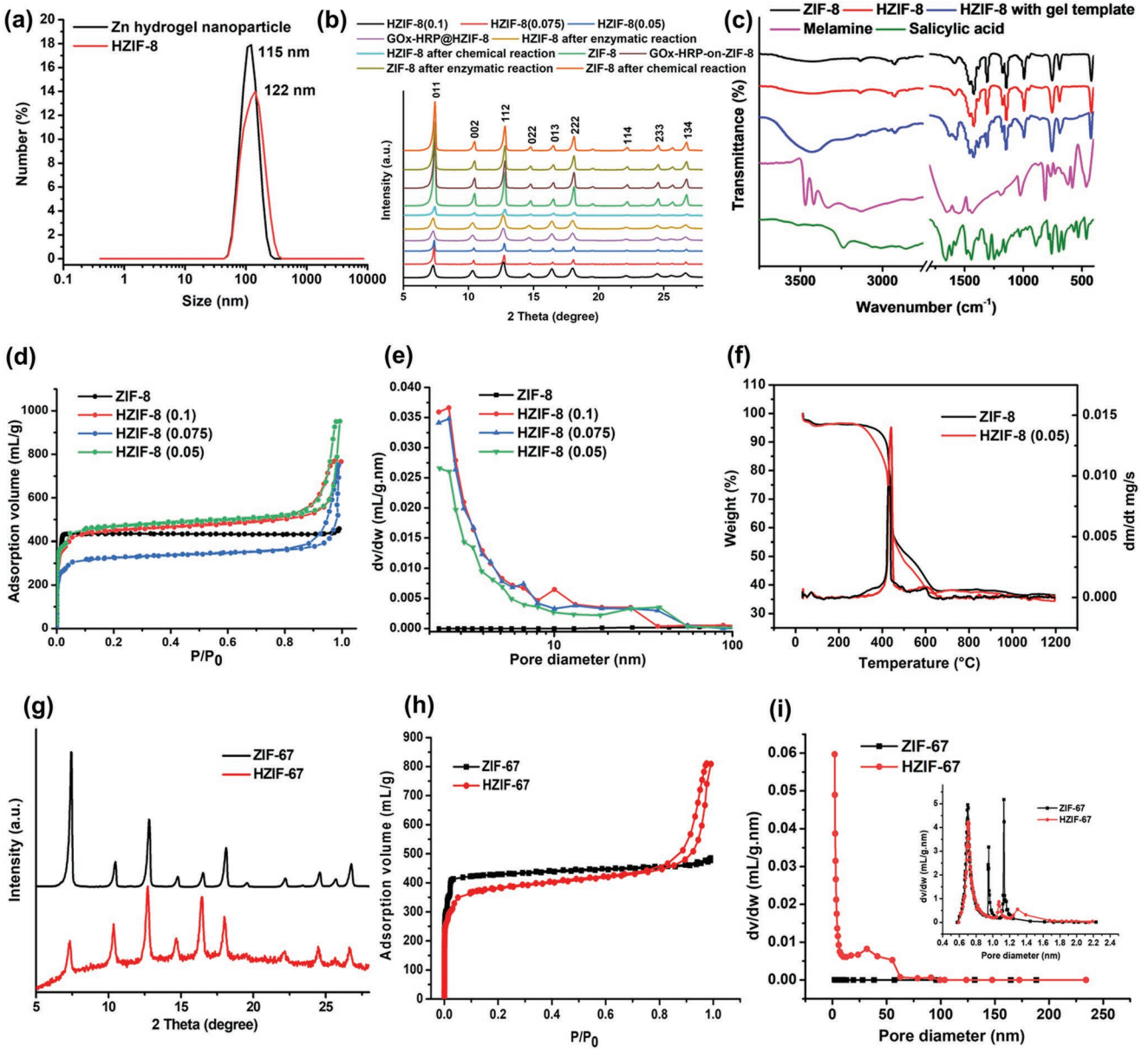

Figure 3. a) Dynamic light scattering of Zn hydrogel nanoparticle and HZIF-8; b) powder X-ray diffraction patterns of HZIF-8 (0.05), HZIF-8 (0.075), HZIF(0.1), ZIF-8, GOx-HRP@HZIF-8(0.1), GOx-HRP-on-ZIF-8, and HZIF-8 and ZIF-8 after enzymatic and chemical reactions; c) FTIR spectra of ZIF-8, HZIF-8, HZIF-8 with gel template, melamine, and salicylic acid; d) nitrogen adsorption/desorption isotherms of HZIF-8 (0.05), HZIF-8 (0.075), HZIF-8 (0.1), and ZIF-8; e) pore size distributions of HZIF-8 (0.05), HZIF-8 (0.075), HZIF-8 (0.1), and ZIF-8; f) thermal gravimetric analysis of ZIF-8 and HZIF-8 (0.05); g) PXRD of HZIF-67 and ZIF-67; h) nitrogen adsorption/desorption isotherms of HZIF-67 and ZIF-67; and i) pore size distributions of HZIF-67 and ZIF-67.

were also characterized. Although the HZIFs-8 had the same XRD patterns (Figure 3b), their porous properties and surface morphologies were distinct. As the N_2 adsorption/desorption isotherms and pore size distributions in Figure 3d,e revealed, the average mesopore size increased from 16.2 to 27.5 nm with the zinc concentration decreased from 0.1 to 0.05 mol L^{-1}. The corresponding Brunauer–Emmett–Teller (BET) surface area decreased from 1431.4 to 1030.1 m^2 g^{-1}. We could also clearly identify the mesopores in HZIFs-8 in the TEM image presented in Figure 2a,c,d. Note that one HZIFs-8 nanoparticle contained only one mesopore. Moreover, with the decrease in zinc concentration, the morphology of HZIF-8 nanocrystals also changed gradually from spherical to cubic. It is known that triethylamine and ammonia are usually used as the deprotonation agent to induce the rapid crystallization of ZIF-8. In our work, melamine, which is abundant with amine functionalities, was used as the component of hydrogel template. This excess of amine groups can cause the difference in HZIF-8 morphology when the zinc concentration was varied.[63] We also compared the thermal gravimetric analysis (TGA) curves of HZIF-8 (0.05) and conventional ZIF-8 and found that the thermal stability did not vary (Figure 3f). Compared with other templating methods

Table 1. Porous properties of conventional microporous ZIFs and mesoporous HZIFs prepared from solution containing different concentrations of zinc ions.

MOF	Average pore width [nm]		Pore volume [mL g^{-1}]		Surface area [m^2 g^{-1}]
	0–2 nm[a)]	2–50 nm[b)]	0–2 nm[a)]	2–50 nm[b)]	
HZIF-8 (0.05)	0.70	27.51	0.49	0.71	1030.1
HZIF-8 (0.075)	0.70	23.14	0.71	0.82	1483.5
HZIF-8 (0.1)	0.71	16.20	0.67	0.57	1431.4
ZIF-8	0.70	–	0.71	–	1403.3
HZIF-67	0.70	15.60	0.56	0.74	1251.0
ZIF-67	0.70	–	0.86	–	1245.5

[a)]The average micropores width and pore volume of MOFs were calculated using SF method; [b)]The average mesopores width and pore volume of MOFs were calculated using BJH method.

that were used for the preparation of mesoporous MOFs,[47–54] our new hydrogel templating strategy enabled the formation of MOF with larger mesopores with an average diameter ranging from 16.2 to 27.5 nm. This MOF also featured a larger BET surface area and mesopore volume (Table S1, Supporting Information). These properties were highly beneficial for the direct encapsulation of larger-size enzymes since they supported rapid mass transfer for the substrates and enzymes and enabled achieving fast reaction rates. Moreover, our approach allows formation and removal of the hydrogel simply by cooling or heating of the aqueous solution of the components. This approach is simpler, green, and easily manageable even on a large scale.

To demonstrate the versatility of our new strategy, the hierarchical micro- and mesoporous HZIF-67 [$Co(Hmim)_2$] was also obtained using the same preparative approach. We optimized again the concentration of metal nodes and found the optimum Co^{2+} concentration of 0.1 mol L^{-1} as indicated in Figure S6 (Supporting Information). In contrast to the rhombic dodecahedral nanocrystals of conventional ZIF-67 shown in Figure 1f, the as-prepared HZIF-67 featured monodispersed spherical nanoparticles with an average particle size of 115 nm (Figure 1e). The PXRD pattern confirmed the highly crystalline structure that was consistent with that of ZIF-67 (Figure 3g). The nitrogen adsorption/desorption isotherms presented in Figure 3h were the type I for ZIF-67 and the type IV for HZIF-67 confirming the microporous structure of ZIF-67 and mesoporous structure of HZIF-67. Figure 3i shows the pore size distributions of both ZIF-67 and HZIF-7. The HZIF-7 surface area was 1251.0 m^2 g^{-1} and the mesopore volume 0.74 mL g^{-1}.

2.2. Catalytic Activity of the Enzyme Cascade System Immobilized in HZIF-8

The average mesopore size of HZIF-8 (0.1) was 16.2 nm thus being much larger than the dimensions of model enzymes glucose oxidase and horseradish peroxidase that were encapsulated within the mesopores of HZIF-8 (here denoted as GOx-HRP@HZIF-8) mainly through the hydrophobic interactions between the enzyme molecules and the hydrophobic walls of the MOF cages. The single enzyme immobilization capacity of HZIF-8 was found to be 141 and 122 mg g^{-1} for HRP and GOx, respectively (**Table 2**). Not surprisingly, the single enzyme immobilization capacity found for ZIF-8 was only 84 mg g^{-1} for GOx and 105 mg g^{-1} for HRP indicating its much lower affinity as the smaller size of pores of ZIF-8 excluded the large size enzymes from entry. They were adsorbed only on the surface of the crystals. We then studied the effect of GOx/HRP ratio by mixing 0.3 mg GOx and 0.3–1.8 mg HRP in 1 mL 10 mmol L^{-1} phosphate buffer saline pH 7.0 with 25 mg HZIF-8 or ZIF-8 nanoparticles. After incubation at room temperature for 24 h, the immobilized enzymes in MOFs were collected by centrifugation, and the supernatant tested for proteins by high-performance liquid chromatography (HPLC). No enzyme was observed in the supernatant confirming that under these conditions the loaded enzymes were completely immobilized in HZIF-8 or ZIF-8.

We also studied the effects of GOx/HRP ratio on enzymatic activity, and found that the dual enzyme nanosystem with a GOx/HRP ratio of 1:5 generated the highest activity of 101.1 ± 1.4 U mg^{-1} (**Table 3**). For comparison, the microporous ZIF-8 was also used as the solid support for the immobilization of GOx and HRP with a GOx/HRP ratio of 1:5 (here denoted as GOx-HRP-on-ZIF-8). The enzyme activity of GOx-HRP-on-ZIF-8 was 112.0 ± 4.7 U mg^{-1}. In a control experiment, we evaluated the possible catalytic activity of original HZIF-8 and ZIF-8 nanoparticles. No conversion of glucose was observed (Figure S7, Supporting Information).

High-resolution transmission electron microscopy (TEM) images in Figure 2e,f revealed the uniform immobilization of enzymes (dark spots) within the mesopores of HZIF-8 framework. In contrast, the enzymes were aggregated and sparsely adsorbed on the surface in the case of microporous ZIF-8. These results demonstrated that HZIF-8 was a suitable host material that prevented enzyme aggregation and rendered the enzymes more accessible to the substrates. The energy-dispersive X-ray spectroscopy (EDS) mapping of GOx-HRP@HZIF-8 is illustrated in **Figure 4** indicated the successful immobilization of enzymes. Notably, both HZIF-8 and ZIF-8 maintained good crystallinity and topology even after immobilization of enzymes as well as after the catalytic reactions indicating the substantial stability of the MOFs. (Figure 3b). The nitrogen adsorption/desorption isotherms presented in Figure S8a (Supporting Information) confirmed a decrease in BET surface area to 409.3 m^2 g^{-1} in GOx-HRP@HZIF-8 due to partial filling the pores after the encapsulation of the enzymes. The enzymes were mainly included in the mesopores of HZIF-8 as indicated from the pore size distribution curve shown in Figure S8b (Supporting Information).

To further elucidate the effect of immobilization on enzyme activity, the kinetic parameters k_{cat} and K_M for both free enzymes

Table 2. The immobilization capacities of GOx and HRP within HZIF-8 and on ZIF-8.

Immobilization capacity [mg g^{-1}]	GOx	HRP
HZIF-8	122	141
ZIF-8	84	105

Table 3. Activities of GOx and HRP bienzymes immobilized within HZIF-8 and ZIF-8 obtained at different GOx/HRP ratios.

MOF	Bienzyme nanosystems	Activity [U mg^{-1}]
HZIF-8	GOx/HRP (1:1)	65.5 ± 2.1
	GOx/HRP (1:2)	79.2 ± 2.8
	GOx/HRP (1:3)	89.8 ± 4.2
	GOx/HRP (1:4)	93.5 ± 3.5
	GOx/HRP (1:5)	101.1 ± 1.4
	GOx/HRP (1:6)	95.5 ± 2.1
ZIF-8	GOx/HRP (1:5)	112.0 ± 4.7

and enzymes immobilized using HZIF-8 (0.1) and ZIF-8 were studied. The activity was assessed using the oxidation of glucose and 2,2′-azino-bis(3-ethylbenzothiazoline-6-sulfonic acid) (ABTS) substrates to the corresponding ABTS■$^{+}$ product monitored at 405 nm. As shown in **Table 4** and Figure S9 (Supporting Information), the apparent K_m decreased for the immobilized enzymes presumably due to the accumulation of more substrates by the MOF scaffolds.[64] In particular, GOx-HRP@HZIF-8 exhibited a much lower K_m value of 2.08×10^{-3} M suggested that HZIF-8 captured more substrates thanks to its mesoporous structure. The decrease in k_{cat} of immobilized enzymes indicated the possible loss of enzyme activity during the immobilization process. But the decreased K_m favored enzyme displaying high catalytic efficiency. As a result, GOx-HRP@HZIF-8 exhibited a significantly higher k_{cat}/K_m value of 85.68 mM s^{-1}, which was 7.7-fold and 2.7-fold higher compared to that found for the free enzymes in solution and GOx-HRP-on-ZIF-8, respectively. These values verified the remarkably enhanced enzyme catalytic efficiency enabled by the large pore sizes of the support that captured more substrates and facilitated the diffusion of both substrate and product molecules. Similar findings have also been discovered by other researchers.[64–67] For example, Yang et al. co-immobilized GOx and HRP at the surface of magnetic nanoparticles by DNA-directed immobilization, and its k_{cat}/K_m value was 11.8-fold better than that of the free enzymes.[66] In another work reported by the same group, the k_{cat}/K_m value of immobilized enzymes was approximately twice of free GOx&HRP.[67]

2.3. Operational Stability of the Enzyme Cascade System Immobilized in HZIF-8

The operational stability of immobilized enzymes was also evaluated by testing their residual activity compared with free

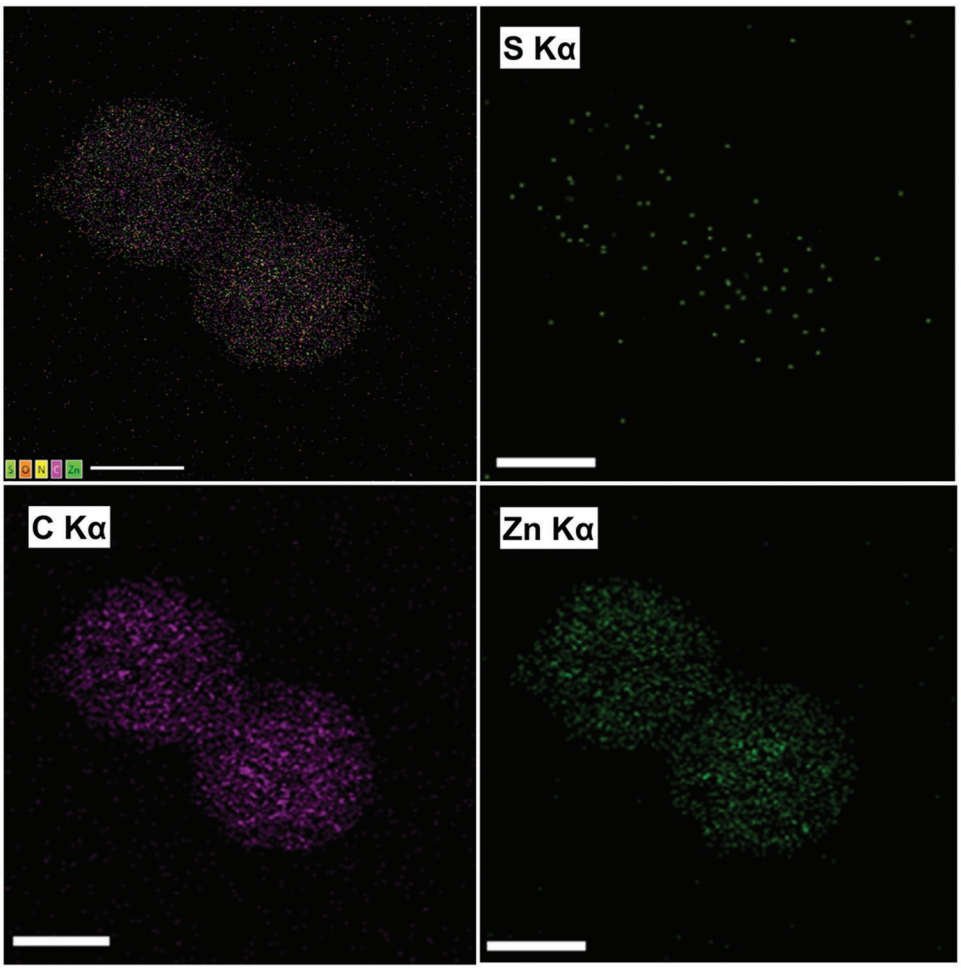

Figure 4. Energy-dispersive X-ray spectroscopy (EDS) analysis of GOx-HRP@HZIF-8(0.1). (Scale bar, 100 nm).

Table 4. Kinetic parameters of cascade reaction catalyzed by free and immobilized enzymes.

Catalyst	K_m [mM]	k_{cat} [s^{-1}]	k_{cat}/K_m [mM s^{-1}]
Free GOx-HRP	21.3	236.89	11.12
GOx-HRP@HZIF-8	2.08	178.22	85.68
GOx-HRP-on-ZIF-8	6.95	219.56	31.59

enzymes in solution after incubation at denaturing conditions including temperature (45, 65, and 95 °C) and pH (2 and 9) for 1 h (**Figure 5**a,b). The enzymes in solution lost 80 and 100% of their initial activities at temperatures of 65 and 95 °C as opposed to 66.7 and 95.5% losses for GOx-HRP-on-ZIF-8, and only 41.6 and 72.5% losses were observed for GOx-HRP@HZIF-8. Regarding conditioning at acidic and basic pH values for 1 h, GOx-HRP@HZIF-8 maintained up to 50 and 65.6% of their initial activity, whereas the residual activities of GOx-HRP-on-ZIF-8 and free enzymes were only 33.7 and 14.5% at pH 2, and 32 and 19.9% at pH 9. These results confirmed that GOx-HRP@HZIF-8 maintained exceptionally high stability under harsh conditions since the mesoporous HZIF-8 support provided an environment that was favorable to preserve protein folding thus retaining the enzyme activity. However, the enzymes that were only adsorbed at the surface of microporous ZIF-8 crystals did not experience the protection effect of the host material, and as a result, the operational stability of GOx-HRP-on-ZIF-8 was significantly reduced.

The reusability of immobilized enzymes was also tested by repeatedly catalyzing reaction of 2 mL solution containing 15 mmol L^{-1} glucose and 30 mmol L^{-1} ABTS as substrates under the same reaction conditions. Figure 5c demonstrates

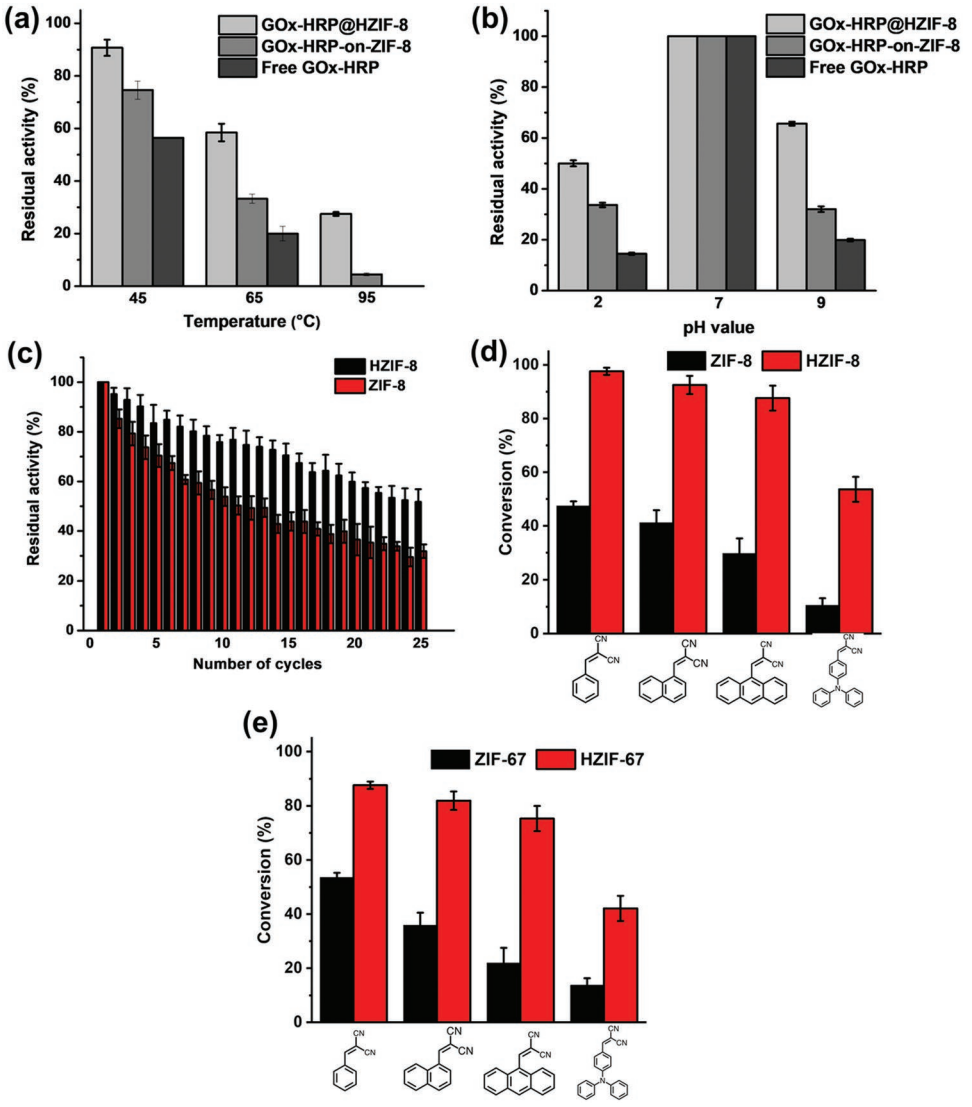

Figure 5. Operational stability of GOx-HRP@HZIF-8 (0.1) in comparison with GOx-HRP-on-ZIF-8 and free enzymes in solution a) at different temperatures (40, 65, and 95 °C) and b) at different pH values (2, 7, and 9), c) reusability of GOx-HRP@HZIF-8 (0.1) and GOx-HRP-on-ZIF-8 with respect to the number of reaction cycles in which the conjugates were used, d) comparison of the derivatives conversions catalyzed by HZIF-8 and ZIF-8, and e) comparison of the derivatives conversions catalyzed by HZIF-7 and ZIF-7.

that GOx-HRP@HZIF-8 again exhibited much higher operational stability with a glucose conversion of 51.7% even after 25 repeated cycles. However, the residual activity of enzymes immobilized on the surface of microporous ZIF-8 retained only 31.8% of their initial activities after the same number of cycles.

2.4. Catalytic Performance in the Knoevenagel Reaction

The catalytic properties of HZIF-8 were also demonstrated with catalysis of Knoevenagel reaction between benzaldehyde derivatives including benzaldehyde, 1-naphthaldehyde, 9-anthracenecarboxaldehyde, and 4-(*N*,*N*-diphenylamino)benzaldehyde, and malononitriles as model substrates.[55,68] As expected, the HZIF-8 was notably more active catalyst compared to microporous ZIF-8. The conversion of the reaction catalyzed by the former ranged from 53.6 to 97.6% while it was only 10.5 and 47.4% upon the catalysis with the latter (Figure 5d). ^{1}H NMR and mass spectra in Figures S10 and S11 (Supporting Information) confirmed the successful synthesis of the target products. XRD patterns in Figure 3b demonstrated that even the chemical reactions did not change the high crystallinity of both HZIF-8 and ZIF-8.

We also compared the catalytic properties of HIZF-67 and ZIF-67 with catalysis of the same Knoevenagel reactions. Here again, the HZIF-67 displayed increased catalytic activity with a conversion ranging from 42.1 to 87.6%, whereas a substrate conversion between 13.7 and 53.5% was achieved with the microporous ZIF-67 (Figure 5e). These results clearly demonstrate the advantages of mesopores that facilitated the accessibility of the reactive sites.

3. Conclusions

We have developed for the first time a new strategy enabling successful preparation of hierarchical micro- and mesoporous ZIFs using hydrogel as template, and demonstrated their superior properties as solid supports for multienzyme immobilization and as catalysts of chemical reactions. The remarkably enhanced enzymatic activity as well as improved operational stability confirm the great potential of mesoporous MOFs serving as a new category of host matrix material for immobilization of enzymes potentially useful in industrial applications. Our ongoing work focuses on the development of new mesoporous MOFs by exploring alternative templates and assembling diverse inorganic, organic, and biological hybrid enzymatic systems designed for the cell-free biosynthesis.

4. Experimental Section

Synthesis of Hierarchical Micro- and Mesoporous ZIF-8 (HZIF-8): Zn hydrogel was prepared by adding 0.05–0.12 mol L^{-1} zinc nitrate in solution of 1.89 mol L^{-1} melamine and 1.89 mol L^{-1} salicylic acid in 20 mL water. The mixture was stirred at 300 rpm and kept at 70 °C for 15 min. A 20 mL hot Zn hydrogel aqueous solution was then added to 80 mL hexane as the oil phase containing 5.0 g Span 85 surfactant. The emulsification was carried out at 60 °C for 1 h using magnetic stirring at 600 rpm, followed by moving the container in the ice bath while stirring the contents at 400 rpm for 30 min to promote the gelation. Finally, 1 mol L^{-1} aqueous 2-methylimidazole solution was added to the emulsion and stirring at 25 °C continued for another 12 h. The as-prepared MOF containing hydrogel was collected by centrifugation and suspended in water at 70 °C for 6 h to remove the hydrogel template. The final HZIF-8 was obtained by centrifugation and repeated washing with ethanol followed by drying under vacuum at 80 °C for 12 h before use.

Synthesis of Hierarchical Micro- and Mesoporous ZIF-67 (HZIF-67): To obtain HZIF-67, cobalt nitrate was used to prepare aqueous hydrogel solution. Further procedures were identical with those described above.

Supporting Information

Supporting Information is available from the Wiley Online Library or from the author.

Acknowledgements

The authors gratefully acknowledge the financial supports from National Natural Science Foundation of China (3181101638, 21861132017, 21576017, 21436002), the National Key Research and Development Program of China (2018YFA0902200), and the Higher Education and High-Quality and World-Class Universities.

Conflict of Interest

The authors declare no conflict of interest.

Keywords

chemical catalysis, enzyme immobilization, hydrogel templates, mesoporous, metal–organic frameworks

Received: June 4, 2019
Revised: August 8, 2019
Published online:

[1] I. W. Bogorad, C.-T. Chen, M. K. Theisen, T.-Y. Wu, A. R. Schlenz, A. T. Lam, J.-C. Liao, *Proc. Natl. Acad. Sci. USA* **2014**, *111*, 15928.
[2] T. Jaroentomeechai, J. C. Stark, A. Natarajan, C. J. Glasscock, L. E. Yates, K. J. Hsu, M. Mrksich, M. C. Jewett, M. P. DeLisa, *Nat. Commun.* **2018**, *9*, 2686.
[3] A. S. Karim, J. T. Heggestad, S. A. Crowe, M. C. Jewett, *Metab. Eng.* **2018**, *45*, 86.
[4] T. P. Korman, P. H. Opgenorth, J. U. Bowie, *Nat. Commun.* **2017**, *8*, 15526.
[5] J. P. Oza, H. R. Aerni, N. L. Pirman, K. W. Barber, C. M. Haar, S. Rogulina, M. B. Amrofell, F. J. Isaacs, J. Rinehart, M. C. Jewett, *Nat. Commun.* **2015**, *6*, 8168.
[6] J. A. Rollin, J. M. del Campo, S. Myung, F. Sun, C. You, A. R. Bakovic, Castro, S. K. Chandrayan, C.-H. Wu, W. W. A. Michael, S. S. Ryan, Y. H. P. Zhang, *Proc. Natl. Acad. Sci. USA* **2015**, *112*, 4964.
[7] Y. H. P. Zhang, *Biotechnol. Adv.* **2015**, *33*, 1467.
[8] K. Petroll, D. Kopp, A. Care, P. L. Bergquist, A. Sunna, *Biotechnol. Adv.* **2019**, *37*, 91.
[9] K. M. Wilding, S. M. Schinn, E. A. Long, B. C. Bundy, *Curr. Opin. Biotechnol.* **2018**, *53*, 115.

[10] C. Bernal, K. Rodríguez, R. Martínez, *Biotechnol. Adv.* **2018**, *36*, 1470.
[11] O. Barbosa, C. Ortiz, Á. Berenguer-Murcia, R. Torres, Rodrigues, R. C. R. Fernandez-Lafuente, *Biotechnol. Adv.* **2015**, *33*, 435.
[12] S. Ding, A. A. Cargill, I. L. Medintz, J. C. Claussen, *Curr. Opin. Biotechnol.* **2015**, *34*, 242.
[13] R. C. Rodrigues, C. Ortiz, Á. Berenguer-Murcia, R. Torres, R. Fernández-Lafuente, *Chem. Soc. Rev.* **2013**, *42*, 6290.
[14] A. Liese, L. Hilterhaus, *Chem. Soc. Rev.* **2013**, *42*, 6236.
[15] X. Lian, Y. Fang, E. Joseph, Q. Wang, J. Li, S. Banerjee, C. Lollar, X. Wang, H.-C. Zhou, *Chem. Soc. Rev.* **2017**, *46*, 3386.
[16] S. L. James, *Chem. Soc. Rev.* **2003**, *32*, 276.
[17] J. R. Long, O. M. Yaghi, *Chem. Soc. Rev.* **2009**, *38*, 1213.
[18] Z. Wang, S. M. Cohen, *Chem. Soc. Rev.* **2009**, *38*, 1315.
[19] D. J. Tranchemontagne, J. L. Mendoza-Cortés, M. O'Keeffe, O. M. Yaghi, *Chem. Soc. Rev.* **2009**, *38*, 1257.
[20] J. R. Li, R. J. Kuppler, H.-C. Zhou, *Chem. Soc. Rev.* **2009**, *38*, 1477.
[21] C. A. Trickett, A. Helal, B. A. Al-Maythalony, Z. H. Yamani, K. E. Cordova, O. M. Yaghi, *Nat. Rev. Mater.* **2017**, *2*, 17045.
[22] N. S. Bobbitt, M. L. Mendonca, A. J. Howarth, T. Islamoglu, J. T. Hupp, O. K. Farha, R. Q. Snurr, *Chem. Soc. Rev.* **2017**, *46*, 3357.
[23] J. R. Li, J. Sculley, H.-C. Zhou, *Chem. Rev.* **2012**, *112*, 869.
[24] J. Lee, O. K. Farha, J. Roberts, K. A. Scheidt, S. T. Nguyen, J. T. Hupp, *Chem. Soc. Rev.* **2009**, *38*, 1450.
[25] L.-B. Sun, X. Q. Liu, H.-C. Zhou, *Chem. Soc. Rev.* **2015**, *44*, 5092.
[26] L. E. Kreno, K. Leong, O. K. Farha, M. Allendorf, R. P. Van Duyne, J. T. Hupp, *Chem. Rev.* **2012**, *112*, 1105.
[27] P. Horcajada, R. Gref, T. Baati, P. K. Allan, G. Maurin, P. Couvreur, G. Férey, R. E. Morris, C. Serre, *Chem. Rev.* **2012**, *112*, 1232.
[28] W.-L. Liu, N.-S. Yang, Y.-T. Chen, S. Lirio, C.-Y. Wu, C.-H. Lin, H.-Y. Huang, *Chem. - Eur. J.* **2015**, *21*, 115.
[29] S. Patra, T. H. Crespo, A. Permyakova, C. Sicard, C. Serre, A. Chaussé, N. Steunou, L. Legrand, *J. Mater. Chem. B* **2015**, *3*, 8983.
[30] S. Jung, Y. Kim, S.-J. Kim, T.-H. Kwon, S. Huh, S. Park, *Chem. Commun.* **2011**, *47*, 2904.
[31] F. Lyu, Y. Zhang, R. N. Zare, J. Ge, Z. Liu, *Nano Lett.* **2014**, *14*, 5761.
[32] X. Wu, J. Ge, C. Yang, M. Hou, Z. Liu, *Chem. Commun.* **2015**, *51*, 13408.
[33] W.-H. Chen, M. Vázquez-González, A. Zoabi, R. Abu-Reziq, I. Willner, *Nat. Catal.* **2018**, *1*, 689.
[34] E. Gkaniatsou, C. Sicard, R. Ricoux, J.-P. Mahy, N. Steunou, C. Serre, *Mater. Horiz.* **2017**, *4*, 55.
[35] H. An, M. Li, J. Gao, Z. Zhang, S. Ma, Y. Chen, *Coord. Chem. Rev.* **2019**, *384*, 90.
[36] Y. Du, J. Gao, H. Liu, L. Zhou, L. Ma, Y. He, Z. Huang, Y. Jiang, *Nano Res.* **2018**, *11*, 4380.
[37] V. Lykourinou, Y. Chen, X.-S. Wang, L. Meng, T. Hoang, L.-J. Ming, R. L. Musselman, S. Ma, *J. Am. Chem. Soc.* **2011**, *133*, 10382.
[38] Y. Chen, V. Lykourinou, T. Hoang, L.-J. Ming, S. Ma, *Inorg. Chem.* **2012**, *51*, 9156.
[39] Y. Chen, V. Lykourinou, C. Vetromile, T. Hoang, L.-J. Ming, R. W. Larsen, S. Ma, *J. Am. Chem. Soc.* **2012**, *134*, 13188.
[40] Y. Chen, S. Han, X. Li, Z. Zhang, S. Ma, *Inorg. Chem.* **2014**, *53*, 10006.
[41] P. Li, S.-Y. Moon, M. A. Guelta, S. P. Harvey, J. T. Hupp, O. K. Farha, *J. Am. Chem. Soc.* **2016**, *138*, 8052.
[42] P. Li, J. A. Modica, A. J. Howarth, E. Vargas L., P. Z. Moghadam, R. Q. Snurr, M. Mrksich, J. T. Hupp, O. K. Farha, *Chem* **2016**, *1*, 154.
[43] P. Li, Q. Chen, T. C. Wang, N. A. Vermeulen, B. L. Mehdi, A. Dohnalkova, N. D. Browning, D. Shen, R. Anderson, D. A. Gómez-Gualdrón, F. M. Cetin, J. Jagiello, A. M. Asiri, J. F. Stoddart, O. K. Farha, *Chem* **2018**, *4*, 1022.
[44] H. Deng, S. Grunder, K. E. Cordova, C. Valente, H. Furukawa, M. Hmadeh, F. Gándara, A. C. Whalley, Z. Liu, S. Asahina, H. Kazumori, M. O'Keeffe, O. Terasaki, J. F. Stoddart, O. M. Yaghi, *Science* **2012**, *336*, 1018.
[45] L. Feng, S. Yuan, L.-L. Zhang, K. Tan, J.-L. Li, A. Kirchon, L.-M. Liu, P. Zhang, Y. Han, Y. J. Chabal, H.-C. Zhou, *J. Am. Chem. Soc.* **2018**, *140*, 2363.
[46] S. Yuan, L. Zou, J.-S. Qin, J. Li, L. Huang, L. Feng, X. Wang, M. Bosch, A. Alsalme, T. Cagin, H.-C. Zhou, *Nat. Commun.* **2017**, *8*, 15356.
[47] L.-Y. Chou, P. Hu, J. Zhuang, J. V. Morabito, K. C. Ng, Y.-C. Kao, S.-C. Wang, F.-K. Shieh, C.-H. Kuo, C.-K. Tsung, *Nanoscale* **2015**, *7*, 19408.
[48] W. Zhang, Y. Liu, G. Lu, Y. Wang, S. Li, C. Cui, J. Wu, Z. Xu, D. Tian, W. Huang, J. S. DuCheneu, W. D. Wei, H. Chen, Y. Yang, F. Huo, *Adv. Mater.* **2015**, *27*, 2923.
[49] L.-G. Qiu, T. Xu, Z.-Q. Li, W. Wang, Y. Wu, X. Jiang, X.-Y. Tian, L.-D. Zhang, *Angew. Chem.* **2008**, *120*, 9629.
[50] Y.-N. Wu, M. Zhou, B. Zhang, B. Wu, J. Li, J. Qiao, X. Guan, F. Li, *Nanoscale* **2014**, *6*, 1105.
[51] S. C. Junggeburth, K. Schwinghammer, K. S. Virdi, C. Scheu, B. V. Lotsch, *Chem. - Eur. J.* **2012**, *18*, 2143.
[52] S. Cao, G. Gody, W. Zhao, S. Perrier, X. Peng, C. Ducati, D. Zhao, A. K. Cheetham, *Chem. Sci.* **2013**, *4*, 3573.
[53] X. Chen, X. Jiang, C. Yin, B. Zhang, Q. Zhang, *J. Hazard. Mater.* **2019**, *367*, 194.
[54] A. F. Abdel-Magied, H. N. Abdelhamid, R. M. Ashour, X. Zou, K. Forsberg, *Microporous Mesoporous Mater.* **2019**, *278*, 175.
[55] K. Shen, L. Zhang, X. Chen, L. Liu, D. Zhang, Y. Han, J. Chen, J. Long, R. Luque, Y. Li, B. Chen, *Science* **2018**, *359*, 206.
[56] J. Huo, J. Aguilera-Sigalat, S. El-Hankari, D. Bradshaw, *Chem. Sci.* **2015**, *6*, 1938.
[57] N. K. Maddigan, A. Tarzia, D. M. Huang, C. J. Sumby, S. G. Bell, P. Falcaro, C. J. Doonan, *Chem. Sci.* **2018**, *9*, 4217.
[58] W. Liang, R. Ricco, N. K. Maddigan, R. P. Dickinson, H. Xu, Q. Li, C. J. Sumby, S. G. Bell, P. Falcaro, C. J. Doonan, *Chem. Mater.* **2018**, *30*, 1069.
[59] Q. Wang, X. Zhang, L. Huang, Z. Zhang, S. Dong, *Angew. Chem., Int. Ed.* **2017**, *56*, 16082.
[60] F.-S. Liao, W.-S. Lo, Y.-S. Hsu, C.-C. Wu, S.-C. Wang, F.-K. Shieh, J. V. Morabito, L.-Y. Chou, K. C. W. Wu, C.-K. Tsung, *J. Am. Chem. Soc.* **2017**, *139*, 6530.
[61] Y. Hu, H. Kazemian, S. Rohani, Y.-M. Huang, Y. Song, *Chem. Commun.* **2011**, *47*, 12694.
[62] B. Roy, P. Bairi, A. Saha, A.-K. Nandi, *Soft Matter* **2011**, *7*, 8067.
[63] K. Shen, L. Zhang, X.-D. Chen, L.-M. Liu, D.-L. Zhang, Y. Han, J.-Y. Chen, J.-L. Long, R. Luque, Y.-W. Li, B.-L. Chen, *Science* **2018**, *359*, 206.
[64] Z. Li, Y. Ding, S. Li, Y. Jiang, Z. Liu, J. Ge, *Nanoscale* **2016**, *8*, 17440.
[65] Y. Zhu, J. Song, J. Zhang, J. Yang, W. Zhao, H. Guo, T. Xu, X. Zhou, L. Zhang, *Catal. Sci. Technol.* **2018**, *8*, 5217.
[66] J. Song, H. Shen, Y. Yang, Z. Zhou, P. Su, Y. Yang, *J. Mater. Chem. B* **2018**, *6*, 5718.
[67] Y. Yang, R. Zhang, B. Zhou, J. Song, P. Su, Y. Yang, *ACS Appl. Mater. Interfaces* **2017**, *9*, 37254.
[68] L. F. Tietze, *Chem. Rev.* **1996**, *96*, 115.

